The Astrophysical Journal, 865:94 (7pp), 2018 October 1 https://doi.org/10.3847/1538-4357/aadb9c

On the Deceleration and Spreading of Relativistic Jets. I. Jet Dynamics

Paul C. Duffell[1] and Tanmoy Laskar[1,2]
[1] Department of Astronomy and Theoretical Astrophysics Center, University of California, Berkeley, CA 94720, USA; duffell@berkeley.edu
[2] Jansky Fellow, National Radio Astronomy Observatory, 520 Edgemont Road, Charlottesville, VA 22903, USA
Received 2017 October 19; revised 2018 August 6; accepted 2018 August 18; published 2018 September 26

Abstract

Jet breaks in gamma-ray burst (GRB) afterglows provide a direct probe of their collimation angle. Modeling a jet break requires an understanding of the jet spreading process, whereby the jet transitions from a collimated outflow into the spherical Sedov–Taylor solution at late times. Currently, direct numerical calculations are the most accurate way to capture the deceleration and spreading process, as analytical models have previously given inaccurate descriptions of the dynamics. Here (in paper I) we present a new, semi-analytical model built empirically by performing relativistic numerical jet calculations and inferring the relationship between the Lorentz factor, opening angle, and shock radius. We then use the analytical model to calculate the Lorentz factor and jet opening angle as a function of the shock radius and compare to the numerical solutions. Our analytic model provides efficient means of computing synthetic GRB afterglow light curves and spectra, which is the focus of paper II.

Key words: gamma-ray burst: general – hydrodynamics – ISM: jets and outflows – shock waves

1. Introduction

One of the most valuable tools in measuring gamma-ray burst (GRB) jet parameters has been a careful analysis of the afterglow emission, which can be observed immediately after the prompt emission (seconds), and is sometimes detectable for long durations of time (months) at wavelengths across the electromagnetic spectrum (though very early and very late detections are rare). X-Ray observations from *Swift* and *Chandra* have enabled the determination of jet properties through modeling (Sari et al. 1999; Nousek et al. 2006; Racusin et al. 2009; Cenko et al. 2010, 2011; Laskar et al. 2015).

One important feature of the afterglow light curve is the jet break. Roughly speaking, this occurs around the time the opening angle of the jet is of the order the inverse of the jet Lorentz factor ($\Gamma\theta_j \sim 1$). At this time, the light curve steepens for two reasons. First, due to relativistic beaming, at this time it becomes possible for the observer to see the edge of the jet, so the decay of the light curve becomes faster than it would if the GRB were a spherical outflow. Second, around this time the center of the jet comes into causal contact with the edge, and the dynamics no longer proceed as if the jet were spherically symmetric. The jet begins to spread sideways, causing it to sweep up more mass and decelerate faster, until the flow becomes subrelativistic and approaches spherical symmetry. In practice, these two effects are coupled, because the fraction of the jet that is visible depends on the lateral spreading of the jet with time.

A measurement of the jet break time makes it possible to constrain the initial opening angle (θ_0) of the jet, allowing for a determination of the true energy scale. Additionally, inferred rates depend on the fraction of jets that are pointed at us, which is determined by the jet opening angle. Finally, knowing how collimated the jet is may help to constrain properties of the progenitor.

As mentioned above, the jet break is due to two different effects, one observational and one dynamical. The observational effect is straightforward to model, but the dynamical effect is more complicated, as it involves knowing how relativistic jets spread in time, which is a nontrivial question. Intermediate asymptotic solutions have been found for this spreading phase (Gruzinov 2007; Keshet & Kogan 2015), but it is still not clear how relevant these solutions are for realistic jets.

Currently, the best way to model the jet spreading phase is through direct hydrodynamical calculations (Granot et al. 2001; Zhang & MacFadyen 2009; Meliani & Keppens 2010; van Eerten et al. 2010a, 2010b; van Eerten & MacFadyen 2011, 2013; Wygoda et al. 2011; De Colle et al. 2012; Duffell & MacFadyen 2015). By numerically integrating the relativistic fluid equations for a jet with a given initial opening angle, and post-processing this solution with a sufficiently detailed radiative transfer calculation, an accurate GRB afterglow light curve can be obtained. Additionally, this process can be made more efficient by exploiting the inherent scale invariance of both the hydrodynamical equations and the synchrotron emission spectrum (Granot 2012; van Eerten & MacFadyen 2012a). By performing only a handful of numerical calculations for different initial jet opening angles, one spans the entire parameter space of the solutions (De Colle et al. 2012; van Eerten et al. 2012), making it possible to invert the problem and find the best-fit parameters for a given GRB afterglow (Ryan et al. 2015; Zhang et al. 2015), though the parameters can be at best determined up to an inherent deceneracy, see Eichler & Waxman (2005).

However, reliance on numerical models, especially for model fitting, can be computationally intensive, and force users to go along with the assumptions used in post-processing the simulations to derive light curves. Analytic models to describe the jet evolution can be more versatile, and if easily implemented, they are extremely useful. Rhoads (1999) modeled the jet evolution as a coupled system of ordinary differential equations for the jet Lorentz factor and opening angle. Unfortunately, this model has been shown to be inaccurate. One of the signatures of this model is an exponential spreading phase, where the shock spreads rapidly sideways almost immediately after the entire jet is in causal contact. Such a rapid spreading phase has not been seen in

numerical studies (Zhang & MacFadyen 2009; van Eerten et al. 2010a; van Eerten & MacFadyen 2012b). See, however, Wygoda et al. (2011).

Lyutikov (2012) suggested that this discrepancy was due to an inaccurate criterion for when the jet begins to spread, and proposed the new criterion $\Gamma \sim 1/\theta_j^{1/2}$. Granot & Piran (2012) found that the discrepancy between analytical and numerical results could be resolved without such drastic changes to the model, and proposed several model improvements. Various new models were compared with a numerical calculation by De Colle et al. (2012), showing that all of these models were reasonably consistent with this numerical result. However, no clear best-fit model was determined in that study, and the results were only compared with a single numerical calculation, with a fairly wide initial opening angle ($\theta_0 = 0.2$).

In the present study, we build a new semi-analytical model, building upon Rhoads (1999, hereafter R99) and Granot & Piran (2012, hereafter GP12). However, rather than proposing several models and comparing them with a numerical calculation, this study proceeds in the opposite direction. We perform several numerical calculations of jet spreading using a range of jet properties and circumburst density profiles. We then provide a unique analytic model, with dimensionless constants calibrated to match the numerical calculations. The underlying physics of our model is consistent with most of the assumptions of R99 and GP12.

We begin by describing the models of R99 and GP12 in more detail, and incorporating our changes to the equations (Section 2). Next, the numerical method and initial conditions are specified (Section 3), after which best-fit parameters are found by matching our models to full relativistic hydrodynamics calculations (Section 4). The results are summarized in Section 5.

2. Analytical Jet Model

2.1. Four-velocity

The most important improvement of GP12 was to extend the model of R99 to nonrelativistic velocities. To do so, the evolution of the jet is expressed in terms of its four-velocity, $u = \Gamma\beta$, as opposed to its Lorentz factor, Γ. One immediate caveat that arises is that the jet is assumed to be described by a single four-velocity, rather than a range of velocities that vary with radial and angular structure. The model assumes that the deceleration of the jet can be summarized by a single value of u at any given time.

R99 described jet evolution based on energy and momentum conservation arguments of Paczynski & Rhoads (1993). According to these arguments, the jet four-velocity is given by

$$u = \frac{\Gamma_0}{\sqrt{1 + 2\Gamma_0 f + f^2}}, \tag{1}$$

where Γ_0 is the initial Lorentz factor and the quantity f is given by the ratio of swept-up mass, m, to the ejecta mass, M_0,

$$f = m/M_0. \tag{2}$$

However, GP12 noted that momentum conservation cannot be used to determine the jet velocity when the flow becomes spherical, as it is based on the conservation of linear momentum, which is zero for a spherical outflow. At late times, the shock velocity can be estimated using the conservation of energy, assuming the total energy is given by its initial value $E = \Gamma_0 M_0$ (units where $c = 1$ are employed here):

$$u \sim \sqrt{E/m} \sim \sqrt{\Gamma_0 M_0/m} \sim \sqrt{\Gamma_0/f}. \tag{3}$$

This asymptotic form suggests that Equation (1) should be modified. This can be done by adding another factor to compensate in this asymptotic limit. The four-velocity in our model is given by

$$u = \frac{\Gamma_0}{\sqrt{1 + 2\Gamma_0 f + f^2}}\sqrt{1 + f/\Gamma_0}, \tag{4}$$

which now agrees with the Sedov scaling in the spherical, nonrelativistic regime.

2.2. Entrained Mass

A formula must be specified for the mass swept up by the jet, to determine the value of f. R99 suggested

$$f = \frac{1}{M_0}\int_0^r \rho(r')\Omega(r')r'^2 dr', \tag{5}$$

where $\Omega(r)$ is the solid angle subtended by the jet when it has reached radius r. GP12 called this the trumpet model, as it suggests that as the jet spreads, it does not entrain any of the mass that it overtakes by spreading, and a diagram for what mass is swept up by the jet takes on a flared, trumpet-like shape.

GP12 proposed an alternate conical model, which is more consistent with what is seen in the numerical studies. In this case, the mass swept up by the jet consists of all mass between the shock front and $r = 0$ within the cone subtended by the opening angle θ_j. In this scenario, $\Omega(r)$ can be pulled out of the integral, which no longer depends on the history of the jet spreading process

$$f = \frac{\Omega}{M_0}\int_0^r \rho(r')r'^2 dr'. \tag{6}$$

If $\rho = Ar^{-k}$, then

$$f = \frac{\Omega A r^{3-k}}{(3-k)M_0}. \tag{7}$$

In practice, we have found the conical model to be more accurate than the trumpet model. This is consistent with what is seen in the numerical studies; while the jet energy is confined within the opening angle θ_j, there is also a bow shock at larger angles carrying an insignificant fraction of the jet energy, yet still entraining mass from the surrounding medium. The spreading of the jet is a process whereby the energy is redistributed into this bow shock, which has already entrained all the mass between the shock front and the origin at $r = 0$. Thus, we can make the assumption that the amount of mass entrained in the jet does not depend on the history of θ_j with time, only on its value at the given time.

2.3. Dynamics of Spreading

Equations (4) and (7) can be closed by giving θ_j as a function of the Lorentz factor. R99 assumed that the jet expanded as a sound wave, starting at $\theta = \theta_0$ and moving outward at the

sound speed in the observer frame,

$$\theta_j = \theta_0 + \frac{t_{\rm co}}{\sqrt{3}\,r}, \tag{8}$$

where

$$t_{\rm co} = \int dt/\Gamma(t). \tag{9}$$

GP12 extended this model by accounting for the curvature of the shock front,

$$\frac{d\theta}{d\ln r} \sim \frac{1}{\Gamma^{1+a}\theta^a}, \tag{10}$$

where the parameter a is either 0 or 1, depending how the shape of the shock front is modeled. It was found in that study that both choices were reasonably consistent with the numerical result with which they were compared.

To determine how fast a sound wave can propagate along an expanding surface, one can treat it much like a cosmology problem. The Minkowski metric is written down in $2+1$ dimensions (polar coordinates), and restricted to a $1+1$ dimensional surface that is an expanding circle with velocity $dr/dt = v$ (and Lorentz factor Γ):

$$ds^2 = -dt^2 + dr^2 + r^2 d\theta^2 \tag{11}$$

$$= -\frac{1}{\Gamma^2}dt^2 + r^2(t)d\theta^2 \tag{12}$$

$$= -\frac{1}{u^2}dr^2 + r^2 d\theta^2 \tag{13}$$

where $u = \Gamma v$ is the four-velocity. Assuming that light rays propagate along null geodesics with $ds^2 = 0$, this would imply the following relationship, which is consistent with GP12,

$$\frac{d\theta}{d\ln r} = \frac{1}{u}. \quad (\text{GP12},\ a = 0). \tag{14}$$

This equation represents the fastest possible lateral motion allowed by causality. In reality, it should be modified because the jet does not spread at the speed of light. R99 assumed that the jet spreads at the speed of sound, but it may take several sound-crossing times for the jet energy to redistribute itself, so the spreading velocity is left as a free parameter, c_j:

$$\frac{d\theta_j}{d\ln r} = \frac{c_j}{u}. \tag{15}$$

It is possible to derive a closed-form relationship between u and θ during the early spreading phase, using Equations (4), (7), and (15). During the spreading phase, $2\Gamma_0 f \gg 1$, so that Equation (4) can be approximated as

$$u = \sqrt{\frac{\Gamma_0}{2f}}. \tag{16}$$

Taking the exterior derivative of both sides, after algebra one obtains,

$$d\ln u = -\frac{1}{2}d\ln f. \tag{17}$$

Using Equation (7) for f,

$$d\ln u = -\frac{1}{2}(d\ln\Omega + (3-k)d\ln r). \tag{18}$$

Assuming the jet is still narrow, and using the small angle approximation $\Omega = \pi\theta_j^2$, one obtains $d\ln\Omega = 2d\ln\theta_j$, and

$$d\ln u = -d\ln\theta_j - \frac{1}{2}(3-k)d\ln r. \tag{19}$$

Combining with Equation (15) to eliminate r,

$$d\ln u = -d\ln\theta_j - \frac{(3-k)u}{2c_j}d\theta_j. \tag{20}$$

For compactness, we define the dimensionless constant $P_k \equiv (3-k)/(2c_j)$. The relationship between the four-velocity and opening angle is therefore

$$\frac{d\ln u}{d\ln\theta_j} = -1 - P_k\theta_j u. \tag{21}$$

If the spreading is very fast, so that P_k is very small, and the last term is neglected, one is left with $u\theta_j = $ constant, reminiscent of the R99 exponential spreading phase in which $\Gamma \sim 1/\theta_j$. Such a phase can occur, if the product $P_k\theta_j u$ becomes small enough. In practice, for typical initial opening angles such a phase does not occur, as was noted by GP12 (consistent with what has been seen in numerical studies).

Equation (21) can be solved by rewriting it as an equation for $u\theta_j$:

$$\frac{d\ln(u\theta_j)}{d\ln\theta_j} = -P_k\theta_j u, \tag{22}$$

with the solution

$$u = \frac{1/\theta_j}{Q_k + P_k\ln(\theta_j/\theta_0)}, \tag{23}$$

where θ_0 is the initial opening angle of the jet, and Q_k is an arbitrary integration constant, which will be fitted to the numerical results. Q_k determines the time when the jet begins to spread; this occurs when $u = 1/(Q_k\theta_0)$. Before this time, the opening angle of the jet remains at its initial value, $\theta_j = \theta_0$.

For larger opening angles, using $\Omega = 4\pi\sin^2(\theta_j/2)$ instead of $\Omega = \pi\theta_j^2$, the extension of (22) is

$$\frac{d\ln(u\sin(\theta_j/2))}{d\ln\sin(\theta_j/2)} = -P_k u(2\tan(\theta_j/2)), \tag{24}$$

resulting in the solution

$$u = \frac{1/(2\sin(\theta_j/2))}{Q_k + P_k\ln\left(\frac{\csc(\theta_0/2)+\cot(\theta_0/2)}{\csc(\theta_j/2)+\cot(\theta_j/2)}\right)}. \tag{25}$$

However, the difference between this and the approximation of Equation (23) is small, even for large opening angles, so Equation (23) will be used to describe the relationship between u and θ_j.

One final adjustment is made to Equation (23). Numerical calculations have shown that as $\theta_j \to \pi/2$ (assuming a symmetric counter-jet), $u \to 0$. In other words, the flow does not become perfectly spherical at a finite velocity (though it becomes nearly spherical at a finite but typically nonrelativistic velocity). To make the algebra consistent with this fact, a small constant term u_0 is subtracted from Equation (23):

$$u_0 \equiv \frac{2/\pi}{Q_k + P_k\ln(\pi/2\theta_0)}, \tag{26}$$

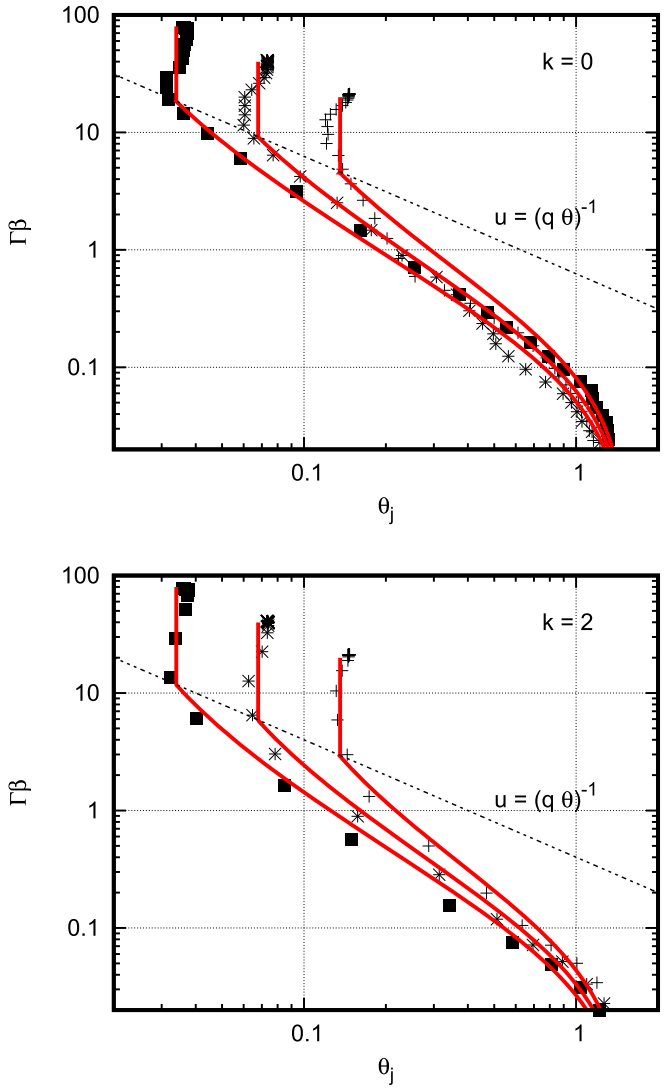

Figure 1. Investigation of the relationship between the Lorentz factor and jet opening angle for various initial conditions. This relationship is well fit by Equation (31). Top panel: jet spreading in the ISM ($k = 0$). Bottom panel: jet spreading in a wind ($k = 2$).

so that

$$u = \frac{1/\theta_j}{Q_k + P_k \ln(\theta_j/\theta_0)} - \frac{2/\pi}{Q_k + P_k \ln(\pi/2\theta_0)}. \quad (27)$$

Note, by assuming a maximal opening angle of $\theta_j \to \pi/2$, we implicitly assume a double-sided jet (and this is also implicitly assumed in the numerical calculations, as we assume mirror symmetry across the equator).

To summarize, the jet evolution can be described by the following four equations:

$$u = \frac{\Gamma_0}{\sqrt{1 + 2\Gamma_0 f + f^2}} \sqrt{1 + f/\Gamma_0}, \quad (28)$$

$$f = \frac{\Omega}{M_0} \int_0^r \rho(r') r'^2 dr', \quad (29)$$

$$\Omega = 4\pi \sin^2(\theta_j/2), \quad (30)$$

$$\theta_j = \begin{cases} \theta_0 & Q_k(u + u_0)\theta_0 < 1 \\ \frac{1/(u+u_0)}{Q_k + P_k \ln(\theta_j/\theta_0)} & \text{otherwise.} \end{cases} \quad (31)$$

Equation (31) is solved iteratively for θ_j, given u (more concretely, Equation (27) is numerically solved for θ_j using Newton's method). In practice, we will find that the constants $Q_k = 1.6$ and $P_k = 2.0$ result in an accurate solution for collision with a wind ($k = 2$), while $Q_k = 2.5$ and $P_k = 4.0$ match well for a deceleration in a uniform density ($k = 0$) medium.

3. Numerical Setup

The constants P_k and Q_k above are measured from the numerical calculations of jet spreading. These numerical calculations are carried out using the JET code (Duffell & MacFadyen 2011, 2013b). The JET code solves the equations of relativistic gas dynamics using a moving mesh. The mesh motion allows for evolution of very high Lorentz factors over many orders of magnitude of expansion.

3.1. Initial Conditions

Initial conditions are given by the boosted fireball model of Duffell & MacFadyen (2013a). This is distinct from the top hat model that is often assumed (other jet structures are also possible, see Zhang & Mészáros 2002). The boosted fireball is parameterized by two Lorentz factors, η_0 and γ_B. The model is found by taking a spherical explosion with Lorentz factor η_0 and boosting to a reference frame moving with relative Lorentz factor γ_B. For ultra-relativistic Lorentz factors, this results in a flow with a total Lorentz factor of $\Gamma_0 \sim 2\eta_0\gamma_B$ and an opening angle of $\theta_0 \sim 1/\gamma_B$. We fix $\eta_0 = 3$ and vary γ_B in our setup, giving a flow with an opening angle of $1/\gamma_B$ and a Lorentz factor $\approx 6\gamma_B$, so that $\Gamma\theta_j \approx 6$ initially.

The jet propagates into the circumburst medium with density, $\rho = Ar^{-k}$. In this study, we concentrate on the cases $k = 2$ (wind) and $k = 0$ (ISM). The initial conditions are set at a very early time such that $ct = 10^{-6}(M_0/A)^{\frac{1}{3-k}}$, where M_0 is the rest mass of the boosted fireball.

3.2. Diagnostics

Measuring jet properties necessitates a reasonable definition for the opening angle θ_j to be measured from the numerical output. Typically, numerical studies use θ_{90}, or the opening angle containing 90% of the jet's energy. Another possible choice is the energy-weighted mean of θ. However, here we use an alternative definition, assuming that as the jet spreads, its energy is redistributed roughly evenly over the given solid angle. From this, one can define the opening angle in terms of the isotropic equivalent energy

$$\Omega = 4\pi E/E_{\rm iso}. \quad (32)$$

As $\Omega = 4\pi \sin^2(\theta_j/2)$,

$$\sin(\theta_j/2) = \sqrt{E/E_{\rm iso}}. \quad (33)$$

$E_{\rm iso}$ is measured by an average of $4\pi dE/d\Omega$ weighted by $dE/d\Omega$:

$$E_{\rm iso} = 4\pi \frac{\int (dE/d\Omega)^2 d\Omega}{\int (dE/d\Omega) d\Omega}. \quad (34)$$

This results in the following formula for θ_j, which is numerically evaluated at each time step as

$$\sin(\theta_j/2) = \frac{E}{\sqrt{4\pi \int (dE/d\Omega)^2 d\Omega}}. \quad (35)$$

This definition has a few benefits over other methods of measuring θ_j: it naturally gives the correct opening angle in the limit of a spherical outflow, and in the limit of a top hat jet structure. It also gives the correct $E_{\rm iso}$ when assuming that the energy is distributed uniformly within θ_j.

The averaged four-velocity is calculated by averaging over all cells, weighted by the energy density:

$$\langle u \rangle = \frac{\int u(r, \theta) \tau dV}{\int \tau dV}. \quad (36)$$

where $\tau = \gamma^2 \rho h - \gamma \rho$ is the energy density after subtracting rest mass energy density. In this expression, γ is the local fluid Lorentz factor, ρ is proper density, and $h = 1 + e + P/\rho$ is the specific enthalpy, where P is the proper pressure and e is specific internal energy.

4. Results

4.1. Measurement of $u(\theta)$

The four-velocity and opening angle are measured at each time step in the numerical calculation, and these values are plotted in Figure 1. Each jet traces out a curve through (u, θ) space, each curve being determined by the initial opening angle, θ_0. These curves are fit to Equation (27) in order to determine the constants P_k and Q_k. The dynamics are reasonably well fit by $P_k = 2.0$, $Q_k = 1.6$, when the jet is colliding with a wind ($\rho \propto r^{-2}$). When the surrounding medium is of uniform density ($\rho = $ const.), the solution is consistent with $P_k = 4.0$, $Q_k = 2.5$.

4.2. Jet Deceleration

Using the analytical equations for u and θ_j (Equations (28)–(31)) along with the appropriate choice of P_k and Q_k, it is now possible to accurately model the evolution of the Lorentz factor with time. Figure 2 shows this evolution for the various initial jet models, showing that the model can accurately reproduce deceleration and spreading of the jet. The deceleration process is recovered in both the $k = 0$ (ISM) and $k = 2$ (wind) cases.

Figure 3 shows that this is a substantial improvement to the model of Rhoads (1999). Using an example with the initial opening angle of $\theta_0 \approx 0.1$ (corresponding to $\eta_0 = 3$, $\gamma_B = 10$) colliding with a wind ($k = 2$), the opening angle and four-velocity as a function of time are compared with the fitted model, alongside the Rhoads model, and a model which ignores the jet's spreading, keeping the opening angle fixed at $\theta_j = \theta_0$. The model is able to accurately reproduce the evolution of θ_j and u with time much better than the Rhoads model because our jet opening angle was fit to numerical calculations, whereas the Rhoads model has no free parameters.

5. Discussion

We have presented a new model for the dynamics of a decelerating and spreading relativistic jet. The model is built from dynamical considerations, and matched to numerical results via two fitting parameters. By performing a survey over initial opening angle θ_0 and density power-law index k, we have shown that the model is broadly effective over the relevant parameter space of GRB and tidal disruption event (TDE) jets.

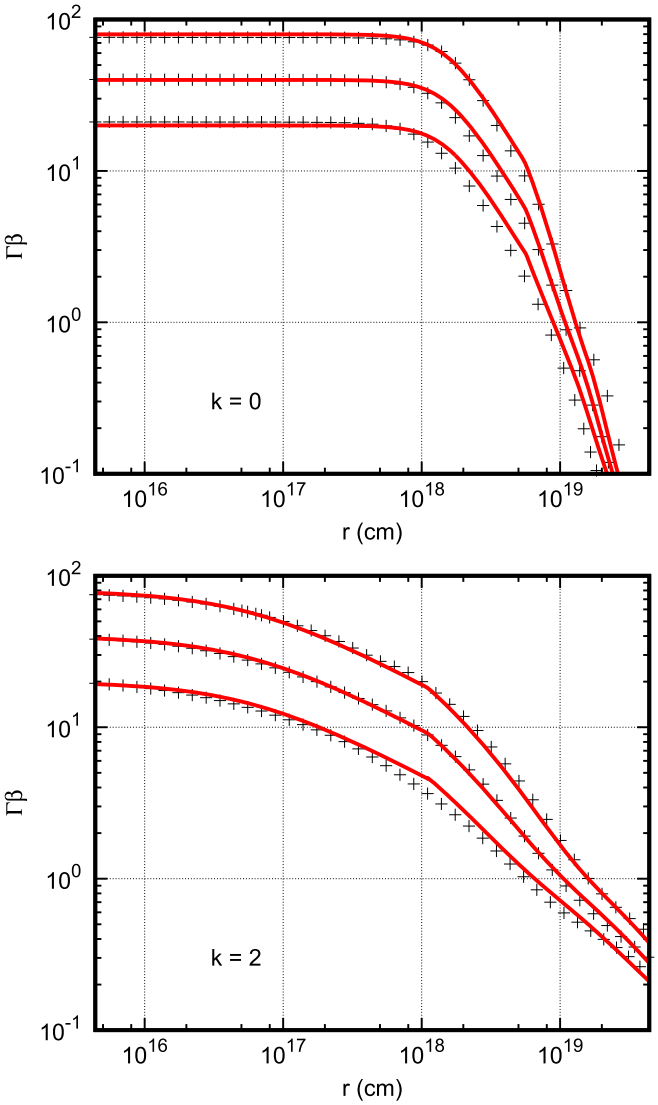

Figure 2. Evolution of the Lorentz factor with time using Equation (28) to determine the spreading of the jet with the opening angle. Top panel: jet spreading in the ISM ($k = 0$). Bottom panel: jet spreading in a wind ($k = 2$). There is a small initial reduction in θ_j seen, due to the nonspherical shape of the initial jet model. The reverse shock points slightly inward as a result, causing a small initial contraction of the flow. The details of this transition may be sensitive to the choice of initial conditions.

The fitted model has been demonstrated to be an improvement to the original model of Rhoads (1999), and is also an improvement to the model of Granot & Piran (2012), as the model is tailored to match with the numerical calculations and is consistent over a significant range of parameter space, including narrow initial opening angles $\theta_0 \sim 0.1$ relevant for GRBs.

The model can be used to construct synthetic light curves and spectra for TDEs and GRB afterglows. This will be the focus of paper II. Because the jet model is analytical, these synthetic observations can be generated rapidly, making it possible to find best-fit jet parameters to the observations.

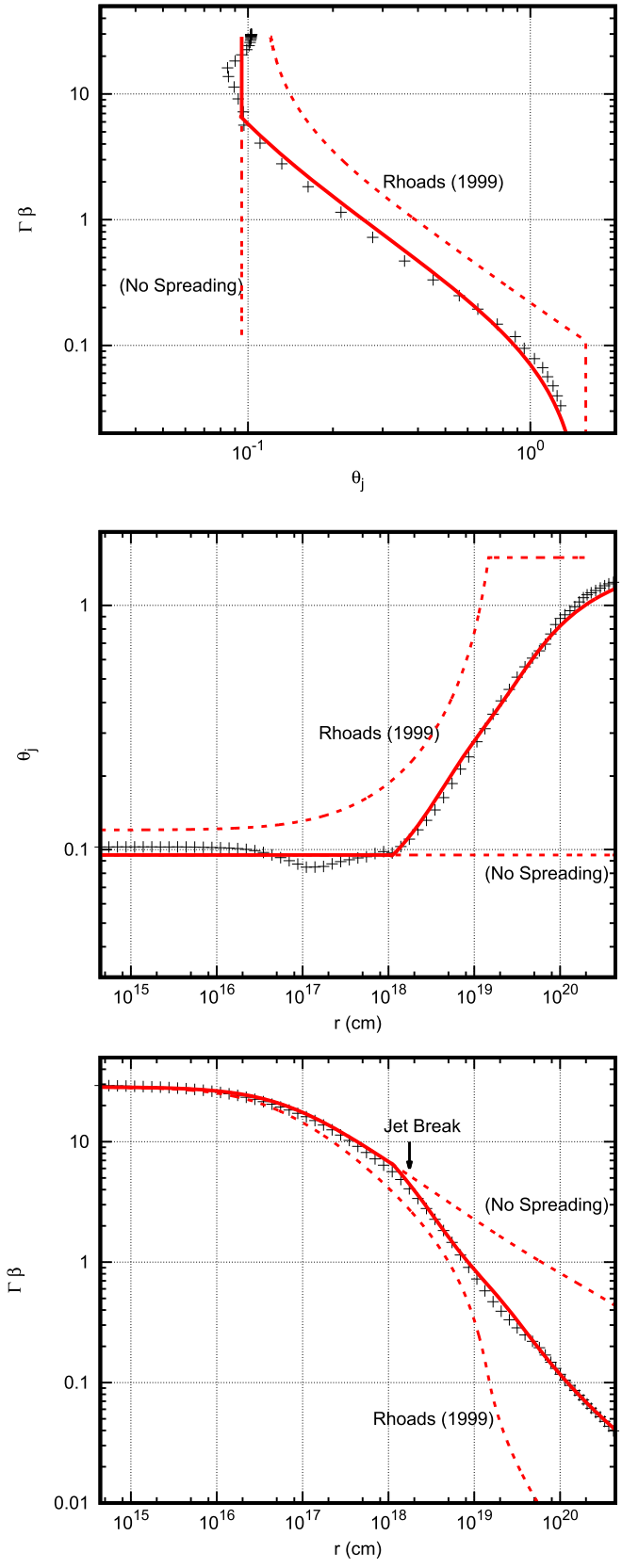

Figure 3. Improvement of the model over Rhoads (1999), for a jet spreading in a wind with the initial opening angle $\theta_0 = 0.1$.

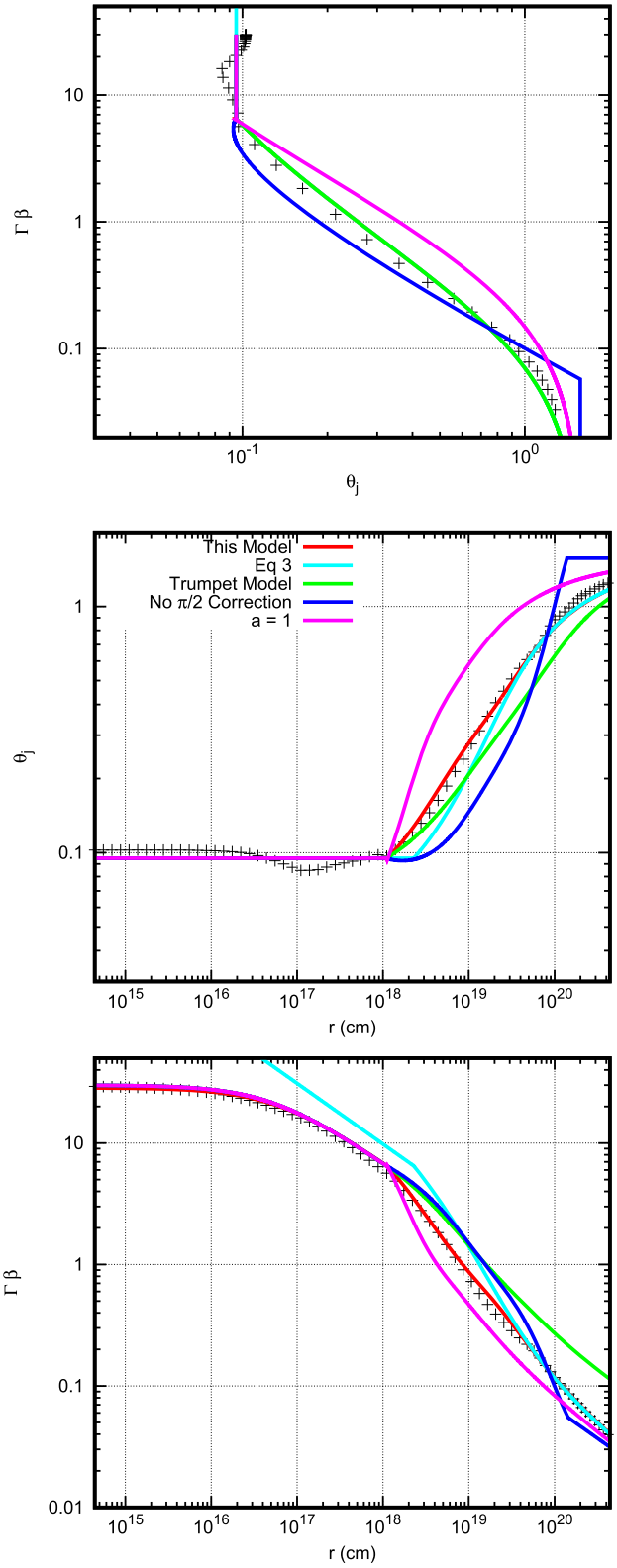

Figure 4. Several different assumptions are tested. The black points are computed from a numerical calculation of a jet with initial opening angle of 0.1 radians colliding with a wind density profile. The red curve is the analytical model presented in this study (cyan and green curves lie exactly on top of this red curve in the top panel). The cyan curve calculates f from Equation (3) rather than Equation (4). The green curve uses the trumpet model to calculate the entrained mass, rather than the conical model. The blue curve is calculated without the $\pi/2$ correction given by the second term in Equation (27). The magenta curve assumes $a = 1$ instead of $a = 0$ in Equation (10).

T.L. is a Jansky Fellow of the National Radio Astronomy Observatory. This work was supported in part by the Theoretical Astrophysics Center at UC Berkeley and by the Gordon and Betty

Moore Foundation through Grant GBMF5076. Early stages of research used the Savio computational cluster resource provided by the Berkeley Research Computing program at the University of California, Berkeley (supported by the UC Berkeley Chancellor, Vice Chancellor of Research, and Office of the CIO). High-resolution calculations were provided by the NASA High-End Computing (HEC) Program through the NASA Advanced Supercomputing (NAS) Division at Ames Research Center.

We would like to thank the anonymous referee for the careful review of our manuscript.

Appendix

Here we briefly sketch out the impact of modifying some of the assumptions made in building the jet model. Figure 4 compares the model presented in this study (red curve) with the numerical data from one of our numerically evolved jets, along with four other analytical models, each one changing a different assumption made in the model presented here.

The cyan curve calculates f from Equation (3) rather than Equation (4). This is to see whether the more complicated form is strictly necessary. While this choice does not affect the relationship between the opening angle and four-velocity, it does affect the early-time behavior, as the deceleration of the jet is not captured in Equation(3); this overpredicts the velocity of the shock during most of the evolution until it has become nonrelativistic.

The green curve uses the trumpet model to calculate the entrained mass, rather than the conical model. This also by itself does not affect the relationship between u and θ_j, but it does cause the jet to sweep up less mass, and decelerate and spread too slowly. This overpredicts the velocity during most of the evolution (except at very early times, when the jet has not significantly decelerated yet).

The blue curve is calculated without the $\pi/2$ correction given by the second term in Equation (27). This term turns out to be quite important, as the spreading process is too fast without this limiting behavior. This might not be an issue for jets that are initially very narrow and that are not observed into the spherical phase, but even for a jet as narrow as $\theta_j = 0.1$ this assumption is significant.

The magenta curve assumes $a = 1$ instead of $a = 0$ in Equation (10). This causes a more rapid spreading of the jet, causing it to decelerate more quickly, underpredicting the velocity after the jet break.

ORCID iDs

Paul C. Duffell https://orcid.org/0000-0001-7626-9629
Tanmoy Laskar https://orcid.org/0000-0003-1792-2338

References

Cenko, S. B., Frail, D. A., Harrison, F. A., et al. 2010, ApJ, 711, 641
Cenko, S. B., Frail, D. A., Harrison, F. A., et al. 2011, ApJ, 732, 29
De Colle, F., Ramirez-Ruiz, E., Granot, J., & Lopez-Camara, D. 2012, ApJ, 751, 57
Duffell, P. C., & MacFadyen, A. I. 2011, ApJS, 197, 15
Duffell, P. C., & MacFadyen, A. I. 2013a, ApJL, 776, L9
Duffell, P. C., & MacFadyen, A. I. 2013b, ApJ, 775, 87
Duffell, P. C., & MacFadyen, A. I. 2015, ApJ, 806, 205
Eichler, D., & Waxman, E. 2005, ApJ, 627, 861
Granot, J. 2012, MNRAS, 421, 2610
Granot, J., Miller, M., Piran, T., Suen, W. M., & Hughes, P. A. 2001, in Gamma-ray Bursts in the Afterglow Era, ed. E. Costa, F. Frontera, & J. Hjorth (Berlin: Springer), 312
Granot, J., & Piran, T. 2012, MNRAS, 421, 570
Gruzinov, A. 2007, arXiv:0704.3081
Keshet, U., & Kogan, D. 2015, ApJ, 815, 100
Laskar, T., Berger, E., Margutti, R., et al. 2015, ApJ, 814, 1
Lyutikov, M. 2012, MNRAS, 421, 522
Meliani, Z., & Keppens, R. 2010, A&A, 520, L3
Nousek, J. A., Kouveliotou, C., Grupe, D., et al. 2006, ApJ, 642, 389
Paczynski, B., & Rhoads, J. E. 1993, ApJL, 418, L5
Racusin, J. L., Liang, E. W., Burrows, D. N., et al. 2009, ApJ, 698, 43
Rhoads, J. E. 1999, ApJ, 525, 737
Ryan, G., van Eerten, H., MacFadyen, A., & Zhang, B.-B. 2015, ApJ, 799, 3
Sari, R., Piran, T., & Halpern, J. P. 1999, ApJL, 519, L17
van Eerten, H., & MacFadyen, A. 2013, ApJ, 767, 141
van Eerten, H., van der Horst, A., & MacFadyen, A. 2012, ApJ, 749, 44
van Eerten, H., Zhang, W., & MacFadyen, A. 2010a, ApJ, 722, 235
van Eerten, H. J., Leventis, K., Meliani, Z., Wijers, R. A. M. J., & Keppens, R. 2010b, MNRAS, 403, 300
van Eerten, H. J., & MacFadyen, A. I. 2011, ApJL, 733, L37
van Eerten, H. J., & MacFadyen, A. I. 2012a, ApJL, 747, L30
van Eerten, H. J., & MacFadyen, A. I. 2012b, ApJ, 751, 155
Wygoda, N., Waxman, E., & Frail, D. A. 2011, ApJL, 738, L23
Zhang, B., & Mészáros, P. 2002, ApJ, 571, 876
Zhang, B.-B., van Eerten, H., Burrows, D. N., et al. 2015, ApJ, 806, 15
Zhang, W., & MacFadyen, A. 2009, ApJ, 698, 1261